# Synthesis and Single-Molecule Conductances of Neutral and Cationic Indenofluorene-Extended Tetrathiafulvalenes: Kondo Effect Molecules

Mads Mansø,[†] Max Koole,[‡] Maarten Mulder,[‡] Ignacio J. Olavarria-Contreras,[‡] Cecilie Lindholm Andersen,[†] Martyn Jevric,[†] Søren Lindbæk Broman,[†] Anders Kadziola,[†] Ole Hammerich,[†] Herre S. J. van der Zant,*[,‡] and Mogens Brøndsted Nielsen*[,†]

[†]Department of Chemistry, University of Copenhagen, Universitetsparken 5, DK-2100 Copenhagen Ø, Denmark
[‡]Kavli Institute of Nanoscience, Delft University of Technology, Lorentzweg 1, 2628 CJ Delft, The Netherlands

S *Supporting Information*
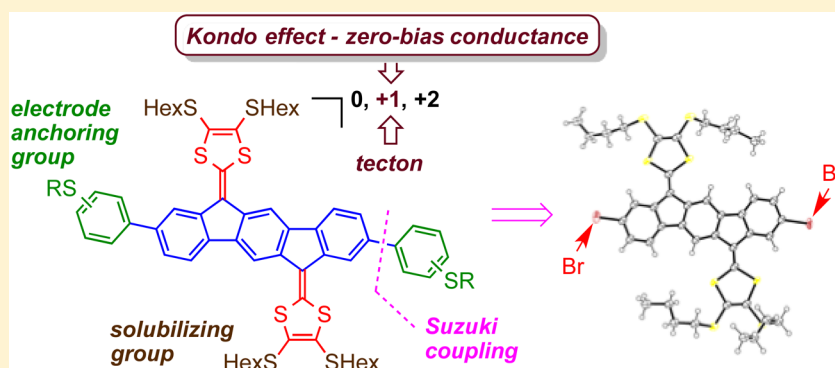
ABSTRACT: Development of molecules that can switch between redox states with paired and unpaired electrons is important for molecular electronics and spintronics. In this work, a selection of redox-active indenofluorene-extended tetrathiafulvalenes (IF-TTFs) with thioacetate end groups was prepared from a readily obtainable dibromo-functionalized IF-TTF building block using palladium-catalyzed cross-coupling reactions, such as the Suzuki reaction. The end groups served as electrode anchoring groups for single-molecule conductance studies, and the molecules were subjected to mechanically controlled break-junction measurements with gold contacts and to low-bias charge transport measurements in gated three-terminal electromigration junctions. The neutral molecules showed clear conductance signatures, and somewhat surprisingly, we found that a *meta−meta* anchoring configuration gave a higher conductance than a *para−meta* configuration. We explain this behavior by "through-space" coupling between the gold electrode and the phenyl on which the anchoring group is attached. Upon charging the molecule in a gated junction, we found reproducibly a Kondo effect (zero-bias conductance) attributed to a net spin. Ready generation of radical cations was supported by cyclic voltammetry measurements, revealing stepwise formation of radical cation and dication species in solution. The first oxidation event was accompanied by association reactions as the appearance of the first oxidation peak was strongly concentration dependent.

INTRODUCTION

Systematic studies of single-molecule conductance as a function of molecular structure are important for the development of suitable molecular wires and switches for molecular electronics.[1] We have in the past few years focused attention on cruciform-like motifs based on an oligo(phenyleneethynylene) (OPE) backbone and an extended tetrathiafulvalene (TTF) as the orthogonal unit.[2,3] Molecule **1** shown in Figure 1 presents one such example. It contains acetyl-protected thiolate end groups, which after deacetylation act as electrode-anchoring groups. Conducting-probe AFM measurements on self-assembled monolayers of such an OPE3-TTF cruciform molecule showed a significantly increased conductance relative to the related OPE3 molecule, while no significant differences

were observed in their single-molecule conductances measured by mechanically controlled break-junction (MCBJ) or scanning tunneling microscopy break-junction (STM-BJ) experiments, and thus, some care has to be taken when comparing results obtained from different methods.[3] An OPE5-TTF cruciform was studied in a three-terminal device,[4] which revealed Kondo effects of the various charge states, that is, zero-bias conductance peaks, signaling the presence of unpaired electrons. For example, a spin-1/2 Kondo effect arises from one unpaired electron, and the Kondo conductance is accompanied by a spin-flip of this electron. This effect is, for
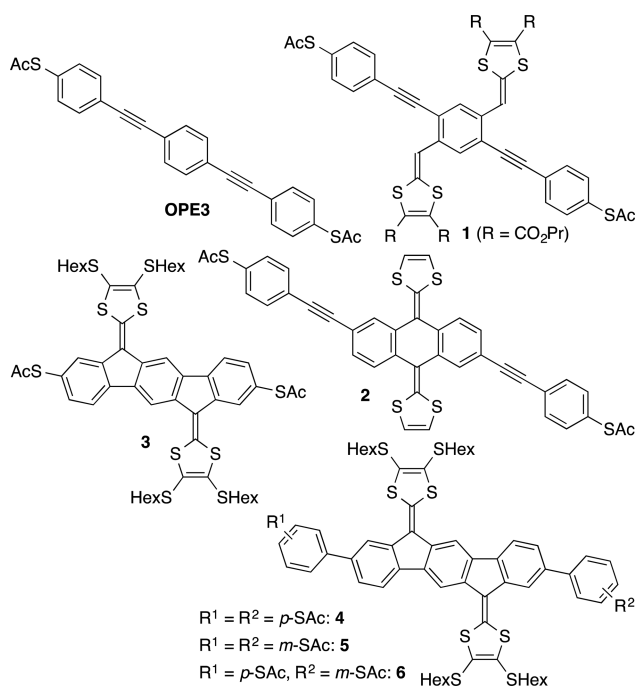
Figure 1. Molecular wires.

example, of importance for developing switchable devices based on organic molecules for spintronics applications. Organic molecules are attractive, as small variations in the molecular structures can have detrimental consequences for the properties. Discovery of an unconventional Kondo effect in redox-active cyclopyrroles[5] and the finding that the paramagnetism of the polychlorotriphenylmethyl radical molecule is preserved in two- and three-terminal solid-state devices, displaying a robust Kondo effect, present examples that have further paved the way for use of organic radicals for spintronics applications, such as magnetic data storage.[6]

One could imagine significant changes in single-molecule conductances of neutral and charged species by having the dithiafulvene units directly part of the backbone of the molecular wire via the exocyclic carbon of the fulvene. García et al.[7] have recently prepared and subjected one such compound, the extended TTF **2** (Figure 1), to STM-BJ measurements, but no clear conductance signature of the neutral molecule was observed, which was explained by either a too low conductance or a reluctance to form a stable junction. Instead, its charge-transfer complex with the 2,3,5,6-tetrafluoro-7,7,8,8-tetracyanoquinodimethane acceptor gave clear conductance signatures. A related series of extended TTFs based on a central indeno[1,2-*b*]fluorene (IF) were recently developed by some of us,[8] and we became interested in elucidating the single-molecule conductances of such molecules, which in contrast to the anthraquinone-based extended TTFs (such as **2**) are planar π-systems and undergo stepwise one-electron oxidations. To do so, synthetic protocols for regioselectively functionalizing the IF-TTF core with suitable electrode anchoring groups had to be developed.

Here, we present the synthesis and MCBJ measurements of IF-TTF derivatives **3**−**6** by incorporating thioacetate end groups in different arrangements; indeed, for these planar molecules clear conductance signatures are observed. Steigerwald, Nuckolls, Venkataraman, and co-workers[9] have recently discussed "through-bond" coupling via *para*-substituted end

groups and "through-space" coupling via *meta*-substituted end groups, and for this reason, we decided to study the three different thioacetate end group combinations: *para*−*para* (**4**), *meta*−*meta* (**5**), and *para*−*meta* (**6**). In addition, we present studies of two of the molecules in a gated three-terminal device, which were performed to elucidate the possibility for generating spin-1/2 Kondo systems upon one-electron oxidation. Formation of the radical cation is for the rigid IF-TTF molecules expected to predominantly place the unpaired, delocalized electron within the backbone of the molecular wire in contrast to our previously studied OPE5-TTF cruciform where the dithiafulvene units are not bridging the phenylene rings of the backbone (Figure 2). Indeed, calculations and ESR studies on
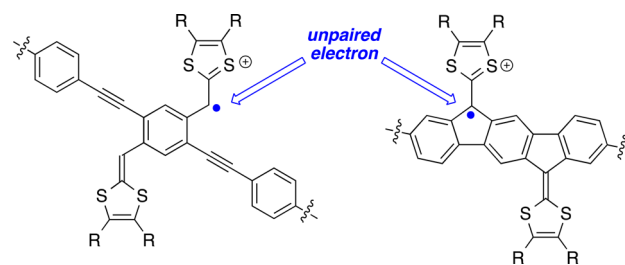

Figure 2. Radical cations of OPE-TTF (left) and IF-TTF (right) cruciform molecules. The unpaired electron is mainly for the IF-TTF part of the backbone of the molecular wire.

the radical cation of IF-TTF have revealed the unpaired electron to be delocalized in the IF core.[8] As a consequence, we hoped to achieve a reproducible and controllable Kondo effect of the charged species, which indeed, turned out to be the case.

■ RESULTS AND DISCUSSION

Synthesis and X-ray Crystal Structure Characterization. Synthetically, we decided to target a dibromo-functionalized IF-TTF that could serve as a substrate for Pd-catalyzed cross-coupling reactions as a means to incorporate the anchoring groups. First, the known bromo-functionalized dione **7**[10] and the phosphonate ester **8a** (prepared in analogy to related compounds[8,11]) were subjected to a double Horner−Wadsworth−Emmons reaction, using sodium hexamethyldisilazide (NaHMDS) as base, to give the bromo-substituted IF-TTF **9a** in a yield of 75% (Scheme 1). The butylthio derivative **9b** was prepared in a similar manner from phosphonate ester **8b**,[11b] but its solubility was too low for further reactions. Compound **9a** was instead a key building block for further functionalizations as shown in Scheme 2. A Pd-catalyzed reaction with potassium thioacetate under microwave heating

Scheme 1. Synthesis of Key Building Block[a]
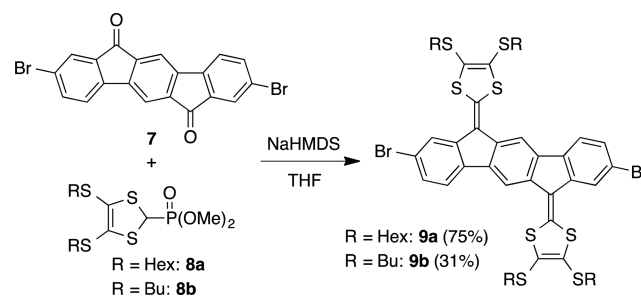
[a]NaHMDS = sodium hexamethyldisilazide.

Scheme 2. Synthesis of Molecular Wires with Thioacetate End Groups[a]
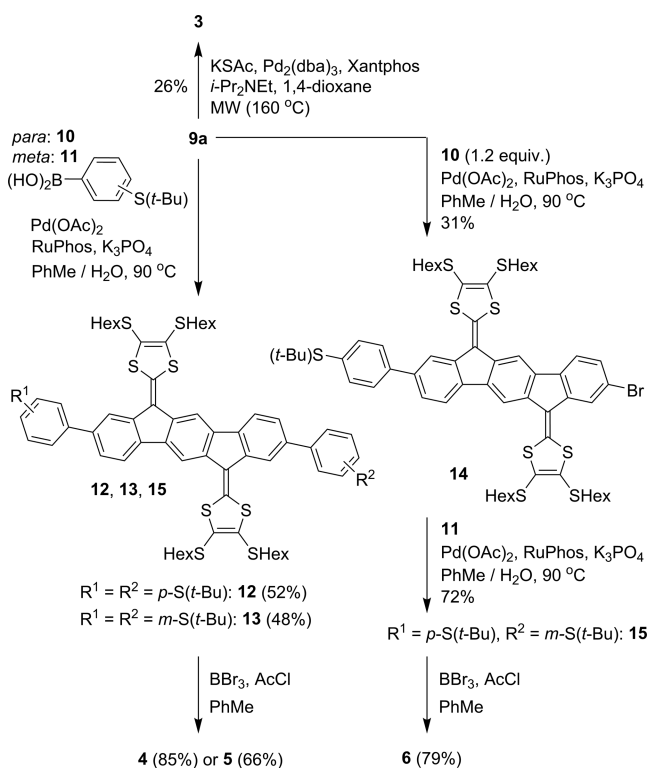
[a] dba = dibenzylidene acetone; Xantphos = 4,5-bis-(diphenylphosphino)-9,9-dimethylxanthene; RuPhos = 2-dicyclohexylphosphino-2′,6′-diisopropoxybiphenyl.

gave the product **3** in a yield of 26% with SAc attached directly onto the core. This is a fair yield considering the complexity of the molecule and the fact that two couplings are performed. Subjecting instead **9a** to Suzuki cross-coupling reactions with either (*p*-(*tert*-butylthio)phenyl)boronic acid (**10**) or (*m*-(*tert*-butylthio)phenyl)boronic acid (**11**) gave the thioethers **12** and **13**, respectively. These compounds were then subjected to boron tribromide and acetyl chloride, which furnished the products **4** and **5** in good yields. By using only 1.2 molar equiv of **10** in the Suzuki cross-coupling of **9a**, the monoadduct **14** could be isolated in a yield of 31% along with **9a** (21%) and **12** (29%). Subjecting this monoadduct to another Suzuki cross-coupling with **11** gave the asymmetric product **15** in good yield, which was finally converted into **6** by the action of boron tribromide and acetyl chloride. Single crystals of compound **9b** were grown from CH$_2$Cl$_2$/heptane and subjected to X-ray crystallographic analysis. The structure is shown in Figure 3, revealing a completely planar IF-TTF π-system.

UV−vis Absorption Spectroscopy. The UV−vis absorption spectra of IF-TTFs **3−6** are shown in Figure 4. They all show a longest-wavelength absorption maximum between 484 and 489 nm in CH$_2$Cl$_2$ with high molar absorptivities.

Electrochemistry. The cyclic voltammograms of **9a** and **4** at different concentrations are shown in Figure 5. Both compounds show two reversible one-electron oxidations accompanied by association reactions. The first oxidation event exhibits a clear concentration dependence, with the peak being broad at high concentrations while sharpening somewhat at low concentration. This behavior is ascribed to the formation of intermolecular complexes, that is, mixed valence dimers (IF-
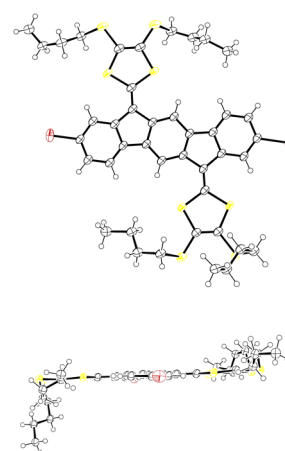

Figure 3. Molecular structure of **9b** (two different views). Ellipsoids are shown at 50% probability for non-H atoms. CCDC 1455260.

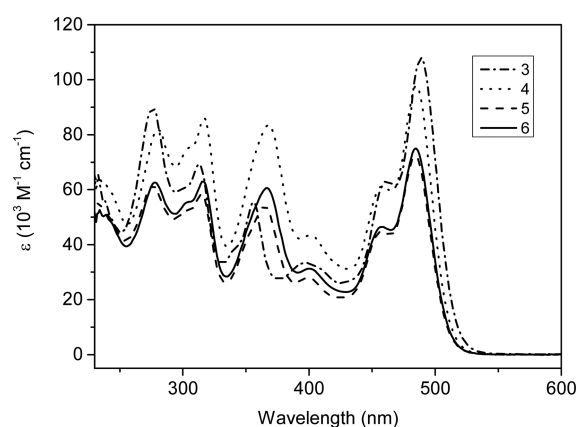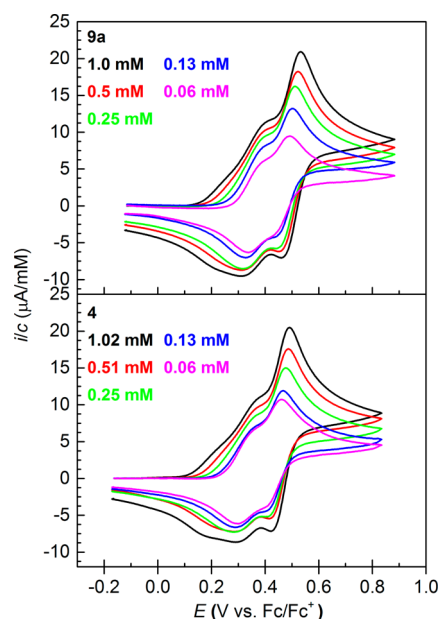**Figure 4.** UV−vis absorption spectra of **3−6** in CH$_2$Cl$_2$.

Figure 5. Cyclic voltammograms of **9a** (top) and **4** (bottom) in CH$_2$Cl$_2$ + 0.1 M Bu$_4$NPF$_6$ recorded at a glassy-carbon working electrode at different concentrations.

TTF)$_2$$^{•+}$ and π-dimers (IF-TTF)$_2$$^{2+}$, as observed previously for related IF-TTF compounds.[8] The two oxidations correspond to

generation of the radical cation and dication species, respectively. It is worth noting that the reversible oxidations experienced by 9a and 4 contrast the behavior of the previously reported OPE-TTF cruciforms.[3] The radical cations of the latter most likely undergo radical dimerization reactions as known[12] to occur for dithiafulvenes where the exocyclic carbon does not have two substituent groups as in the IF-TTFs.

Mechanically Controlled Break-Junction Experiments.
The conductances of IF-TTFs 3−6 were measured at room temperature using a mechanically controlled break-junction setup. The devices consist of a phosphorus bronze flexible substrate coated with a polyimide insulation layer on top of which a lithographically patterned gold wire with a constriction is evaporated. The narrower part of the wire is suspended by reactive ion etching of the polyimide. The substrate is then clamped at both ends and bent by the action of a pushing rod beneath the center of the substrate until the gold wire breaks, leaving two atomically sharp electrodes separated by a nanoscale gap. In the case where no molecule bridges the gap, the breaking traces show a featureless exponential conductance decrease indicative of single-barrier tunneling. If a molecule contacts both electrodes, the conductance no longer follows this behavior. Instead, a slower conductance decay with steplike features is observed.

Figure 6 displays the two-dimensional conductance vs electrode displacement histograms of the compounds. The
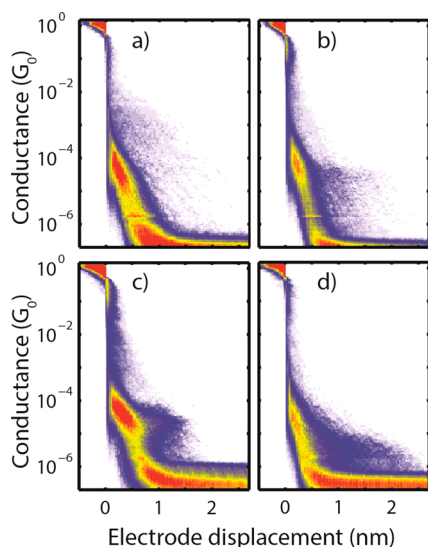

Figure 6. Two-dimensional conductance vs electrode displacement histograms constructed from 5000 individual traces of compounds 3, 4, 5, and 6 (a, b, c, and d, respectively). The molecules were drop-casted from a 0.5 μM solution in CH_2Cl_2; a concentrated solution of tetrabutylammonium hydroxide (Bu_4NOH) in CH_2Cl_2 was used to cleave the acetyl group to form the thiolate end group. The bias voltage was 0.1 V, and the electrode speed was 6 nm/s.

histograms show an accumulation of counts in the region from 0 to 0.5 nm of displacement dropping from around $10^{-4}G_0$ to the noise level of about $10^{-7}G_0$, where G_0 is the conductance quantum ($= 2e^2/\hbar$ with $\hbar$ the Plank constant and e the charge of an electron ($2e^2/\hbar = 77$ μS)). This behavior corresponds to that expected for single-barrier tunneling involving junctions, in which no molecule bridges the electrodes after the gold contacts snap apart. On top of this signal, regions can be identified in which the conductance vs displacement traces are

show steplike features at characteristic conductance values; these traces are attributed to molecular junctions. The yield for these traces is approximately 5−20% depending on the specific molecule; this is typical for these types of MCBJ experiments.[13]

To obtain the most probable conductance values of the compounds, one-dimensional histograms are constructed, and in the regions of conductance where plateau features are observed, a log-normal distribution has been fitted through the data. In the cases in which no clear peak could be identified due to a low yield of junction formation or because the plateaus were close to the noise level, partial histograms were constructed using selection criteria detailed in the SI. The conductance values of different samples are summarized in Table 1.

Table 1. Most Probable Conductance Values for Compounds 3−6 Extracted from a Log-Normal Fitting of the Conductance Histograms (See the SI, Figure S2)[a]

molecule	conductance (G_0)		
	sample 1	sample 2	sample 3
3	2.1×10^{-4b}	1.4×10^{-4b}	
4	3.4×10^{-5}	2.8×10^{-5}	2.8×10^{-5}
5	1.4×10^{-5}	1.5×10^{-5}	2.1×10^{-5}
6	2.1×10^{-6b}	1.4×10^{-6b}	

[a]Measurements have been performed on two samples for compounds 3 and 6 and on three different samples for compounds 4 and 5. [b]Values obtained after data selection as described in the SI.

Compound 3 is the shortest of the molecules and shows the highest conductance. Its value is similar to what we find for OPE3 ($1.35 \times 10^{-4}G_0$),[3,14] which has the same anchoring groups and is a π-conjugated molecule of similar length. This result reflects the importance of the coplanarity of the indenofluorene and dithiafulvene units in contrast to the butterfly-like shape of the previously studied extended TTF 2, for which no clear conductance signatures could be found.[7] For the other IF-TTFs, somewhat surprisingly, the conductance values decrease in the following sequence: 4 (*para−para*) > 5 (*meta−meta*) > 6 (*para−meta*). Thus, compound 5 with two *meta*-contacted benzene rings at its ends has a higher conductance than 6 with one *para* benzene ring as the end group. This is somehow unexpected since one expects the *meta−meta*-configured molecule to have a lower conductance due to quantum interference effects.[15] Possibly, in that case, a considerable amount of junctions are formed in such a configuration that injection into the molecular backbone not only occurs through the sulfur atoms but also directly in the π-system of the ring itself. We note that high conductances of other *para−meta* wires have been explained in this way.[9]

Three-Terminal Conductance Experiments. To investigate low-bias charge transport through IF-TTFs with *meta−meta* (5) and *para−meta* (6) thioacetate end groups, three-terminal electromigration junctions[16] were used. They consist of a lithographically fabricated gold nanowire, deposited on a chip, with an aluminum oxide-covered gate electrode. The nanowire is controllably electromigrated in solution (dichloromethane containing 0.1 mM of compound 5 or 6) at room temperature down to a resistance of 5 KΩ. The junctions are then allowed to self-break to form a nanogap; this procedure avoids the formation of gold grains in the gap. When the resistance of the junctions is of the order of 1 MΩ, the junctions are cooled in vacuo to cryogenic temperatures (for

further details, see the SI). Current−voltage characteristics for both samples as a function of gate voltage and magnetic field are shown in the SI. Figure 7 shows the differential conductance map of charge transport as a function of bias and gate voltage (left panels) as well as magnetic field (right panels).
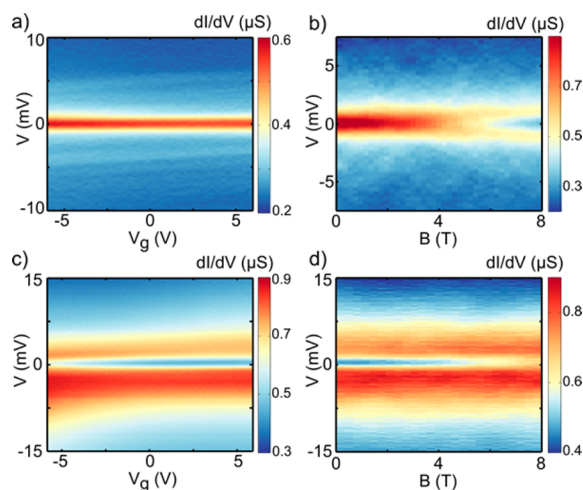

Figure 7. Differential conductance (dI/dV) map of charge transport in electromigrated junctions as a function of bias (V), gate (V_g) voltage, and magnetic field (B). (a) dI/dV map (at $T = 2.2$ K) of compound **5** showing a zero-bias peak spanning the entire gate range. The peak broadens slightly for negative gate voltages. (b) dI/dV (taken at $V_g = 6$ V and $T = 2.2$ K) as a function of magnetic field of the zero-bias peak in (a). Zero-bias peak splits for increasing magnetic field (Zeeman effect). (c) dI/dV map (at $T = 2.5$ K) of compound **6** showing a peak with a suppression at zero-bias. The shape of the feature changes slightly as a function of gate voltage. (d) dI/dV (taken at $V_g = 0$ V and $T = 2.5$ K) as a function of magnetic field for the feature in (c). The dip disappears with increasing magnetic field.

Multiple samples with compound **5** or **6** were measured. In the data, two recurring features could be identified. One feature is a zero-bias peak (red line in Figure 7a), which splits as a function of magnetic field (Figure 7b) and decays nonlinearly as a function of increasing temperature (SI, Figure S6). The second feature is the appearance of a broad peak with a suppression at zero-bias (Figure 7c). The suppression disappears as a function of magnetic field (Figure 7d) and shows a non-monotonic temperature dependence (SI, Figure S6). The occurrence of enhanced conduction at and around zero-bias with the observed dependence on temperature and magnetic field suggests that both features are related to Kondo correlations formed by a net spin on the molecule in the junctions. A single spin on the molecules can explain the zero-bias peaks observed by means of the formation of a spin-1/2 Kondo system.[17] However, parts c and d of Figure 7 show features which can be related to two unpaired electrons, where the singlet and triplet configurations of the two electrons are nearly degenerate.[18] Full degeneracy of the singlet and triplet configurations may therefore result in a single peak in conductance as in parts a and b of Figures 7.

A significant amount of electromigrated junctions with compounds **5** and **6** present transport features mediated by a spin-degree of freedom. Both compounds show these features with a yield of approximately 20% compared to successfully electromigrated junctions (24% and 17% for compounds **5** and

6, respectively; however, this difference is statistically not significant). As compounds **5** and **6** inherently do not possess an unpaired spin, it suggests that the interaction of the molecules with a surface (source, drain, or gate electrodes) forms unpaired spins in the compounds, most likely due to oxidation of the redox-active DTF units. A possible mechanism for this could be via image charges effects in the electrodes.[19]

For the radical cations in the electromigrated junctions, the conductances are almost 2 orders of magnitude higher than those measured for the assumingly neutral molecules in the mechanically controlled break-junctions. When compared to previous measurements on TTF derivatives, studied in various set-ups,[20] a higher conductance is indeed expected for the oxidized species, but one has to be careful in comparing the conductances between our two set-ups as the junction geometries (presence of the gate, the dielectric, and the shape of the electrodes) are different (and, in principle, charging of the molecules in the mechanically controlled break-junctions cannot be excluded).

CONCLUSIONS

In conclusion, we have developed efficient synthetic protocols for thioacetate end-capped IF-TTF molecular wires using a readily obtainable IF-TTF with two bromo substituents as a key building block for Pd-catalyzed cross-coupling reactions. Single-molecule conductance measurements reveal that for these molecules a "through-space" coupling seems to be in play when the anchoring group is placed in a *meta*-configuration as a higher than expected conductance was observed for the *meta*−*meta* anchored wire. Two of the molecules were investigated in gated three-terminal junctions, where they exhibited conductance features around zero-bias, which were attributed to Kondo correlations due to unpaired spins. In all, this work has shown that IF-TTFs comprise a class of extended TTFs, which are interesting not only as tectons for supramolecular chemistry on account of their reversible and sequential one-electron oxidations and strong cation associations (neutral·cation and cation·cation), allowing for redox-controlled assembly, but also as molecular wires for molecular electronics with Kondo effect behavior that can be achieved routinely. While redox-active derivatives of TTF have been extensively studied in molecular electronics, this is only the second example in which Kondo-effect behavior has been established and the first example on how this behavior is controlled by placing the unpaired electron within the wire itself of an extended TTF. The reproducibility obtained by this molecular design paves the way for studying spin−spin interactions and associated Kondo effects in a more controlled way.

EXPERIMENTAL SECTION

Electrochemistry. The electrochemical reduction (see SI) and oxidation of **4** and **9a** were studied with cyclic voltammetry (CV) and differential pulse voltammetry (DPV). The concentration of the electroactive solute was 1 mM in dichloromethane (from solvent tower). The scan speed of the CV was 0.1 V s^{-1}, and the step potential and the modulation amplitude of the DPV were 2 and 25 mV, respectively. Compensation of the solution resistance (iR-compensation) was included (900−1000 ohm). The measured potentials have been referenced to the ferrocene/ferrocenium (Fc/Fc$^+$) redox couple, and the supporting electrolyte was a 0.1 M tetra-*n*-butylammonium hexafluorophosphate (Bu$_4$NPF$_6$, ≥99%) solution. For all measurements, a 3 mm diameter glassy-carbon disk was chosen as the working electrode, a Pt wire as the counter electrode, and a Ag wire immersed in the solvent-supporting electrolyte mixture and physically was

separated from the solution containing the substrate by a ceramic frit as the reference electrode. All voltammograms have been recorded under an argon atmosphere. The concentration-dependent measurements were performed by diluting the solute directly in the electrochemical cell, and a background subtraction has been performed before plotting.

Mechanically Controllable Break-Junction Technique. Single-molecule conductance measurements were performed in a mechanically controllable break-junction (MCBJ) set up. The devices consist of a phosphorus bronze flexible substrate coated with a polyimide insulation layer on top of which a lithographically patterned gold wire with a constriction is evaporated. The narrower part of the wire is suspended by reactive ion etching of the polyimide. The substrate is then clamped at both ends and bent by the action of a pushing rod beneath the center of the substrate until the gold wire breaks leaving two atomically sharp electrodes separated by a nanoscale gap. The electrodes are fused and broken thousands of times at a rate of 6 nm/s. During this process, the conductance ($G = I/V$) is recorded using a logarithmic amplifier with a bias voltage of $V = 0.1$ V. During each breaking process the conductance is recorded as a function of the electrode displacement. Before the gold wire breaks, the conductance of the junction drops in a stepwise manner due to atomic rearrangements in the contact. When the metallic contact breaks, the conductance sharply drops below $1G_0$. This sharp decrease in conductance is used to set the zero displacement of each trace. In the case where no molecule bridges the gap, the break traces show a featureless exponential conductance decrease indicative of single-barrier tunneling. If a molecule contacts both electrodes the conductance no longer follows this behavior. Instead, a slower conductance decay with steplike features is observed. To obtain the most probable conductance values, we construct one-dimensional conductance histograms and fit log-normal distributions in the region of conductance where molecular features were observed (for details, see the SI).

Electromigration Setup. The electromigrated breakjunction experiments were performed using nanofabricated breakjunctions. On a silicon/silicon oxide chip a 90 nm thick Au gate electrode is deposited. The entire chip with gate electrode is covered with 5 nm of atomic layer deposited aluminum oxide. On top of this, in three separate e-beam and evaporation steps, a 10 nm thick Au nanowire, 90 nm thick Au source pads, and a 110 nm thick Au patch to connect the source pads to the nanowire are deposited (see the SI, Figure S3, for an image of a device). Each chip contains 32 breakjunctions, of which 24 are wire bonded in a chip carrier. The chip is loaded in a liquid cell with a solution of dichloromethane containing 0.1 mmol of compound **5** or **6**. Feedback-controlled electromigration is performed in liquid at room temperature. The junctions with a resistance of 100 Ω are electromigrated until the wires are 5 KΩ. After this, the junctions are allowed to self-break in liquid and at room temperature; this is done to minimize the chance of forming spurious gold grains in the junction. When the junction resistances are of the order of 1MΩ (there is a spread of 2−3 orders of magnitude between the junctions), the liquid cell is pumped to high vacuum and cooled to cryogenic temperatures. At cryogenic temperatures, the current through the electromigrated junctions is measured as a function of bias and gate voltage. Furthermore, the setup also possesses a superconducting magnet, a 1 K pot, and heater resistor, which make it possible to perform temperature and magnetic field dependent measurements.

Synthesis and Routine Characterization: General Methods. Anhydrous THF and 1,4-dioxane were obtained by distillation from Na/benzophenone. Anhydrous toluene was distilled from Na. All palladium-catalyzed coupling reactions were carried out under either a nitrogen or an argon atmosphere using solvents flushed with argon for at least 15 min aided by ultrasonification. ^{1}H and ^{13}C NMR spectra were acquired using an instrument with a noninverse cryoprobe at 500 MHz or a pentaprobe at 500 MHz. The residual solvent peak was used as reference (CDCl$_3$: ^{1}H NMR, 7.26 ppm (CHCl$_3$), ^{13}C NMR, 77.16 ppm; C$_6$D$_6$: ^{1}H NMR, 7.16 ppm (C$_6$HD$_5$), ^{13}C NMR, 128.06 ppm). Coupling constants (J) are specified in hertz (Hz). In ^{13}C APT NMR spectra CH and CH$_3$ correspond to negative signals and C and CH$_2$

correspond to positive signals. Flash column chromatography was performed using SiO$_2$ with a particle size of 40−63 μm. CDCl$_3$ for NMR spectroscopy was filtered through Al$_2$O$_3$ prior to use. UV/vis absorption spectra were recorded within the range of 200−1100 nm using a 1 cm quartz cuvette. High-resolution mass spectrometry (HR-MS) was performed on an ESP-MALDI-FT-ICR spectrometer equipped with a 7 T magnet (calibration of the instrument was done with NaTFA cluster ions). When referring to petroleum spirit, a technical grade with boiling point 40−65 °C was used.

*Compound **9b**.* The phosphonate ester **8b** (378 mg, 970 μmol) was dissolved in distilled THF (15 mL) and argon-flushed for 15 min by aid of ultrasonification. The mixture was then cooled to −78 °C, and NaHMDS (1.5 mL, 0.6 M in toluene, 0.9 mmol) was added. After 1 h of stirring, the mixture was transferred via cannula to a suspension of **7** (100 mg, 227 μmol) in distilled THF (15 mL) at −78 °C. The cooling bath was removed, and the mixture was stirred at rt for 20 h. The mixture was poured into saturated ammonium chloride and then extracted with CH$_2$Cl$_2$ (2 × 50 mL). The organic phase was washed with brine, and then the brine was extracted with CS$_2$ (2 × 50 mL). The organic phases were combined and dried over Na$_2$SO$_4$, and the solvent was removed by a flow of nitrogen. Flash column chromatography (SiO$_2$, CS$_2$) gave crude **9b** (90 mg). To the crude was added 10 mL of CH$_2$Cl$_2$, and then the mixture was centrifuged. The mother liquor was removed, and the solid was pure **9b** (68 mg, 71 μmol, 31%). HR-MS (MALDI+ FT-ICR): m/z = 961.9587 [M$^{\bullet+}$], calcd for [C$_{42}$H$_{44}$^{79}Br$_2$^{32}S$_8$$^+$] m/z = 961.9570. ^{1}H NMR (500 MHz, CDCl$_3$): δ = 7.82 (s, 2H), 7.77 (d, J = 1.6 Hz, 2H), 7.63 (d, J = 8.0 Hz, 2H), 7.41 (dd, J = 8.0, 1.6 Hz, 2H), 3.08−2.90 (m, 8H), 1.81−1.68 (m, 8H), 1.61−1.48 (m, 8H), 0.99 (t, J = 7.3 Hz, 12H). ^{13}C NMR (126 MHz, CDCl$_3$): δ = 139.1, 139.1, 136.9, 136.5, 134.7, 129.6, 128.9, 128.2, 125.8, 120.6, 120.6, 119.7, 114.0, 36.6, 36.6, 32.0, 32.0, 22.0, 21.9, 13.9, 13.8. Anal. Calcd for C$_{42}$H$_{44}$Br$_2$S$_8$: C, 52.27; H, 4.60. Found: C, 52.23; H, 4.35.

*Compound **9a**.* To a solution of the phosphonate ester **8a** (413 mg, 0.929 mmol) in dry, degassed THF (16 mL) at −78 °C was added NaHMDS (1.6 mL, 0.6 M in toluene, 0.93 mmol). After being stirred for 1 h at −78 °C, the solution was transferred via cannula to a suspension of the dione **7** in dry argon-flushed THF (16 mL) at −78 °C. The cooling bath was removed, and the mixture was stirred for 22 h before it was poured into saturated aqueous ammonium chloride (100 mL) and extracted with CH$_2$Cl$_2$ (3 × 50 mL). The combined organic phases were washed with brine (50 mL), dried over Na$_2$SO$_4$, and concentrated in vacuo. The crude mixture was subjected to flash column chromatography (SiO$_2$, CS$_2$) and then crystallized from CH$_2$Cl$_2$/heptane to give **9a** as an orange solid (183 mg, 75%). The reaction was repeated on a larger scale (**8a**: 1.00 g, 2.25 mmol) to give **9a** in a yield of 69% (1.69 g). Mp: 177−178 °C. HR-MS (MALDI+ FT-ICR): m/z = 1074.0847 [M$^{\bullet+}$], calcd for [C$_{50}$H$_{60}$^{79}Br$_2$^{32}S$_8$$^+$] m/z = 1074.0822. ^{1}H NMR (400 MHz, CDCl$_3$): δ = 7.73 (d, J = 1.6 Hz, 2H), 7.70 (s, 2H), 7.56 (d, J = 8.1 Hz, 2H), 7.38 (dd, J = 8.1, 1.6 Hz, 2H), 3.07−2.97 (m, 8H), 1.78 (p, J = 7.4 Hz, 8H), 1.55−1.49 (m, 8H), 1.43−1.33 (m, 16H), 0.97−0.90 (m, 12H). ^{13}C NMR (126 MHz, CDCl$_3$): δ = 139.1, 139.0, 136.9, 136.4, 134.6, 129.5, 128.9, 128.2, 125.7, 120.5, 120.5, 119.7, 113.9, 37.0, 36.9, 31.6, 30.0, 28.5, 22.7, 14.2 (5 C's masked). Anal. Calcd for C$_{50}$H$_{60}$Br$_2$S$_8$: C, 55.75; H 5.61. Found: C, 55.62; H, 5.59.

*Compound **3**.* To a flame-dried vial suitable for microwave irradiation were added **9a** (101 mg, 93.8 μmol), Xantphos (10 mg, 10.5 μmol), Pd$_2$(dba)$_3$ (10 mg, 10.9 μmol), and potassium thioacetate (24 mg, 210 μmol), and the vial was then flushed with argon. To the vial was added an argon-flushed solution of i-Pr$_2$NEt (0.1 mL, 0.574 mmol) in freshly distilled 1,4-dioxane (8 mL). The vial was sealed with a lid suitable for high pressure and transferred to a microwave oven, and the mixture was heated to 160 °C for 2.5 h. The mixture was allowed to cool to rt, diluted with water (100 mL), and extracted with CH$_2$Cl$_2$ (3 × 100 mL). The combined organic phases were dried over Na$_2$SO$_4$ and concentrated in vacuo. The solid residue was purified by flash column chromatography (CH$_2$Cl$_2$/heptane, 2:3 to 1:1) to give **3** as an orange solid (26 mg, 26%). Mp: 144−150 °C. HR-MS (MALDI + FT-ICR): m/z = 1066.2264 [M$^{\bullet+}$], calcd for [C$_{54}$H$_{66}$O$_2$S$_{10}$]$^{\bullet+}$ m/z =

1066.2264. ^{1}H NMR (500 MHz, C$_6$D$_6$): δ = 8.27 (s, 2H), 8.23 (d, J = 1.4 Hz, 2H), 7.73 (d, J = 7.8 Hz, 2H), 7.45 (dd, J = 7.8, 1.4 Hz, 2H), 2.79 (t, J = 7.3 Hz, 4H), 2.68 (t, J = 7.3 Hz, 4H), 1.96 (s, 6H), 1.60 (p, J = 7.4 Hz, 4H), 1.53 (p, J = 7.4 Hz, 4H), 1.34−1.04 (m, 24H), 0.87 (t, J = 7.3 Hz, 6H), 0.85 (t, J = 7.3 Hz, 6H). ^{13}C NMR (126 MHz, CD$_2$Cl$_2$): δ 195.2, 139.9, 139.3, 138.6, 137.1, 135.5, 132.1, 129.9, 129.6, 129.2, 126.6, 120.4, 120.0, 114.9, 37.3, 32.0, 30.6, 30.4, 30.4, 28.9, 23.2, 14.4 (5 C's masked). Anal. Calcd for C$_{54}$H$_{66}$O$_2$S$_{10}$: C, 60.75; H, 6.23. Found: C, 60.82; H, 6.19.

Compound 12. To an argon-flushed solution of **9a** (50 mg, 46 μmol) in toluene (25 mL) and water (5 mL) were added RuPhos (9 mg, 19 μmol), K$_3$PO$_4$ (68 mg, 0.32 mmol), (4-(*tert*-butylthio)-phenyl)boronic acid (36 mg, 0.17 mmol), and Pd(OAc)$_2$ (3 mg, 13 μmol). The mixture was heated to 90 °C for 18 h. The mixture was then diluted with water (100 mL) and extracted with CH$_2$Cl$_2$ (2 × 100 mL). The combined organic phases were dried over Na$_2$SO$_4$ and concentrated in vacuo. Flash column chromatography (CH$_2$Cl$_2$/heptane, 3:7) gave **12** as a red solid (30 mg, 52%). Mp: 214−215 °C. HR-MS (MALDI+ FT-ICR): m/z = 1246.3977 [M$^{•+}$], calcd for [C$_{70}$H$_{86}$S$_{10}$]$^{•+}$ m/z = 1246.3931. ^{1}H NMR (500 MHz, CDCl$_3$): δ = 7.80 (d, J = 1.3 Hz, 2H), 7.79 (s, 2H), 7.75 (d, J = 7.8 Hz, 2H), 7.67 (d, J = 8.4 Hz, 4H), 7.64 (d, J = 8.4 Hz, 4H), 7.48 (dd, J = 7.8, 1.3 Hz, 2H), 2.97 (t, J = 7.3 Hz, 4H), 2.94 (t, J = 7.3 Hz, 4H), 1.78−1.69 (zm, 8H), 1.52−1.43 (m, 8H), 1.39 (s, 18H), 1.36−1.28 (m, 16H), 0.92−0.86 (m, 12H). ^{13}C NMR (126 MHz, CDCl$_3$): δ = 142.3, 138.5, 138.3, 138.0, 137.9, 137.1, 136.9, 135.3, 131.5, 128.9, 128.6, 127.3, 124.5, 121.6, 121.0, 119.7, 114.2, 46.3, 36.8, 31.6, 31.5, 31.2, 30.0, 30.0, 28.5, 28.5, 22.7, 22.7, 14.2, 14.2 (1 C masked). Anal. Calcd for C$_{70}$H$_{86}$S$_{10}$: C, 67.37; H, 6.95. Found: C, 67.42; H, 6.84.

Compound 4. To an argon-flushed solution of **12** (111 mg, 88.9 μmol) in toluene (35 mL) was added AcCl (3.5 mL). The mixture was cooled to 0 °C, and BBr$_3$ (0.37 mL, 1 M in CH$_2$Cl$_2$, 0.37 mmol) was added, resulting in a color change to black. After 3 h, the solution was poured onto ice and extracted with CH$_2$Cl$_2$ (3 × 100 mL). The combined organic phases were dried over Na$_2$SO$_4$ and concentrated in vacuo. The crude mixture was purified by crystallization from CHCl$_3$/heptane to give **4** as an orange solid (92 mg, 85%). Mp: >230 °C. HR-MS (MALDI+ FT-ICR): m/z = 1218.2946 [M$^{•+}$], calcd for [C$_{66}$H$_{74}$O$_2$S$_{10}$]$^{•+}$ m/z = 1218.2890. ^{1}H NMR (500 MHz, CS$_2$/C$_6$D$_6$, 1:4): δ = 8.35 (br. s, 2H), 8.12 (br. s, 2H), 7.89 (d, J = 7.8 Hz, 2H), 7.66 (d, J = 8.3 Hz, 4H), 7.48−7.44 (m, 6H), 2.82 (t, J = 7.3 Hz, 4H), 2.74 (t, 4H), 2.00 (s, 6H), 1.68−1.54 (m, 8H), 1.40−1.13 (m, 24H), 0.90−0.83 (m, 12H). ^{13}C NMR (126 MHz, CS$_2$/C$_6$D$_6$, 1:4): δ 191.4, 143.2, 139.3, 139.0, 138.4, 137.9, 137.7, 136.1, 135.2, 139.1, 127.5, 125.5, 122.4, 121.8, 120.3, 115.1, 37.3, 37.1, 32.0, 31.9, 30.4, 29.9, 28.9, 28.9, 23.3, 23.3, 14.6, 14.6 (2 C's masked). Anal. Calcd for C$_{66}$H$_{74}$O$_2$S$_{10}$: C, 64.98; H 6.11. Found: C, 64.87; H, 5.93.

Compound 13. To an argon-flushed solution of **9a** (84 mg, 78 μmol) in toluene (30 mL) and water (7.5 mL) were added RuPhos (22 mg, 47 μmol), K$_3$PO$_4$ (131 mg, 617 μmol), (3-(*tert*-butylthio)-phenyl)boronic acid (61 mg, 0.29 mmol), and Pd(OAc)$_2$ (6 mg, 27 μmol). The mixture was heated to 90 °C for 17 h. The mixture was diluted with water (100 mL) and extracted with CH$_2$Cl$_2$ (2 × 100 mL). The combined organic phases were dried over Na$_2$SO$_4$ and concentrated in vacuo. Flash column chromatography (CH$_2$Cl$_2$/heptane, 3:7) gave **13** as a red solid (47 mg, 48%). Mp: 72−75 °C. HR-MS (MALDI+ FT-ICR): m/z = 1246.3964 [M$^{•+}$], calcd for [C$_{70}$H$_{86}$S$_{10}$]$^{•+}$ m/z = 1246.3931. ^{1}H NMR (500 MHz, CDCl$_3$): δ = 8.02 (s, 2H), 7.92 (dd, J = 1.7, 1.7 Hz, 2H), 7.90 (d, J = 7.9 Hz, 2H), 7.89 (d, J = 1.5 Hz, 2H), 7.70 (ddd, J = 7.6, 1.7, 1.2 Hz, 2H), 7.55 (ddd, J = 7.6, 1.7, 1.2 Hz, 2H), 7.53 (dd, J = 7.9, 1.5 Hz, 2H), 7.45 (t, J = 7.6 Hz, 2H), 3.01 (t, J = 7.4 Hz, 4H), 2.96 (t, J = 7.4 Hz, 4H), 1.80−1.68 (m, 8H), 1.53−1.43 (m, 8H), 1.39 (s, 18H), 1.37−1.29 (m, 16H), 0.90 (t, J = 7.1 Hz, 6H), 0.87 (t, J = 7.1 Hz, 6H). ^{13}C NMR (126 MHz, CDCl$_3$): δ = 142.5, 139.3, 138.4, 137.8, 137.5, 137.2, 136.5, 136.1, 135.5, 133.4, 129.2, 129.0, 127.8, 124.9, 122.0, 121.0, 119.9, 114.5, 46.2, 36.9, 36.8, 31.6, 31.5, 31.2, 30.0, 29.9, 28.5, 28.4, 22.7, 22.7, 14.2, 14.2, 14.2. Anal. Calcd for C$_{70}$H$_{86}$S$_{10}$: C, 67.37; H, 6.95. Found: C, 67.30; H, 6.96.

Compound 5. To an argon-flushed solution of **13** (71 mg, 57 μmol) in toluene (22 mL) was added AcCl (2.3 mL). The mixture was cooled to 0 °C, and BBr$_3$ (0.22 mL, 1 M in CH$_2$Cl$_2$, 220 μmol) was added, resulting in a color change to black. After 9 h, the solution was poured onto ice and extracted with CH$_2$Cl$_2$ (3 × 50 mL). The combined organic phases were dried over Na$_2$SO$_4$ and concentrated in vacuo. The crude mixture was purified by crystallization from CHCl$_3$/heptane to give **5** as an orange solid (46 mg, 66%). Mp: 180−183 °C. HR-MS (MALDI+ FT-ICR): m/z = 1218.2942 [M$^{•+}$], calcd for [C$_{66}$H$_{74}$O$_2$S$_{10}$]$^{•+}$ m/z = 1218.2890. ^{1}H NMR (500 MHz, CS$_2$/C$_6$D$_6$, 1:4): δ = 8.37 (s, 2H), 8.16 (dd, J = 1.5, 0.5 Hz, 2H), 7.92 (dd, J = 1.7, 1.7 Hz, 2H), 7.88 (dd, J = 7.8, 0.5 Hz, 2H), 7.63 (ddd, J = 7.7, 1.7, 1.1 Hz, 2H), 7.48 (dd, J = 7.8, 1.5 Hz, 2H), 7.35 (ddd, J = 7.7, 1.7, 1.1 Hz, 2H), 7.22 (t, J = 7.7 Hz, 2H), 2.81 (t, J = 7.3 Hz, 4H), 2.80 (t, J = 7.3 Hz, 4H), 2.00 (s, 6H), 1.67−1.56 (m, 8H), 1.37−1.15 (m, 24H), 0.87 (t, J = 7.1 Hz, 6H), 0.85 (t, J = 7.2 Hz, 6H). ^{13}C NMR (126 MHz, CS$_2$/C$_6$D$_6$, 1:4): δ 191.8, 143.7, 139.5, 139.1, 138.5, 137.9, 137.9, 136.3, 133.7, 132.9, 130.4, 129.8, 129.6, 128.5, 125.5, 122.6, 121.9, 120.4, 115.1, 37.1, 36.8, 31.9, 31.8, 30.3, 30.2, 29.9, 28.8, 28.7, 23.1, 14.4, 14.4 (2 C's masked). Anal. Calcd for C$_{66}$H$_{74}$O$_2$S$_{10}$: C, 64.98; H, 6.11. Found: C, 64.67; H, 6.11.

Compound 14. To an argon-flushed solution of **9a** (401 mg, 372 μmol) in toluene (70 mL) and water (20 mL) were added RuPhos (20 mg, 43 μmol), K$_3$PO$_4$ (214 mg, 1.01 mmol), (4-(*tert*-butylthio)-phenyl)boronic acid (96 mg, 0.46 mmol), and Pd(OAc)$_2$ (5 mg, 22 μmol). The mixture was heated to 90 °C for 3.5 h. The mixture was diluted with water (200 mL) and extracted with CH$_2$Cl$_2$ (4 × 100 mL). The combined organic phases were dried over Na$_2$SO$_4$ and concentrated in vacuo. Flash column chromatography (CH$_2$Cl$_2$/heptane, 1:3 to 2:3) gave **14** as a red solid (133 mg, 31%). From the flash column chromatography, the products **9a** (83 mg, 21%) and **12** (131 mg, 29%) were also isolated. HR-MS (MALDI+ FT-ICR): m/z = 1160.2374 [M$^{•+}$], calcd for [C$_{60}$H$_{73}$BrS$_9$]$^{•+}$ m/z = 1160.2377. ^{1}H NMR (500 MHz, CDCl$_3$): δ 7.82 (d, J = 1.5 Hz, 1H), 7.76 (d, J = 7.8 Hz, 1H), 7.76 (d, J = 0.6 Hz, 1H), 7.73 (d, J = 0.6 Hz, 1H), 7.70 (d, J = 8.4 Hz, 2H), 7.68 (d, J = 1.7 Hz, 1H), 7.66 (d, J = 8.4 Hz, 2H), 7.52 (d, J = 8.0 Hz, 1H), 7.51 (dd, J = 7.8, 1.5 Hz, 1H), 7.32 (dd, J = 8.0, 1.7 Hz, 1H), 3.01−2.93 (m, 8H), 1.80−1.68 (m, 8H), 1.53−1.45 (m, 8H), 1.39 (s, 9H), 1.36−1.31 (m, 16H), 0.92−0.88 (m, 12H). ^{13}C NMR (126 MHz, CDCl$_3$): δ = 142.3, 138.9, 138.5, 138.5, 138.3, 138.0, 137.8, 137.2, 137.0, 136.9, 136.1, 135.1, 134.6, 131.5, 129.0, 128.7, 128.7, 128.7, 127.9, 127.4, 127.2, 125.6, 124.4, 121.5, 120.8, 120.2, 120.2, 119.8, 119.6, 113.9, 46.3, 36.9, 36.8, 36.8, 31.6, 31.6, 31.5, 31.2, 30.0, 30.0, 30.0, 28.6, 28.5, 28.5, 22.8, 22.8, 22.7, 22.7, 14.2, 14.2, 14.2, 14.2 (4 C's masked).

Compound 15. To an argon-flushed solution of **14** (101 mg, 86.9 μmol) in toluene (30 mL) and water (9 mL) were added RuPhos (10 mg, 21 μmol), K$_3$PO$_4$ (61 mg, 0.29 mmol), (3-(*tert*-butylthio)-phenyl)boronic acid (29 mg, 0.14 mmol), and Pd(OAc)$_2$ (4 mg, 18 μmol). The mixture was heated to 90 °C for 4.5 h. The mixture was diluted with water (100 mL) and extracted with CH$_2$Cl$_2$ (3 × 80 mL). The combined organic phases were dried over Na$_2$SO$_4$ and concentrated in vacuo. Flash column chromatography (CH$_2$Cl$_2$/heptane, 3:7) gave **15** as a red solid (78 mg, 72%). Mp: changes color and becomes a bit oily gradually from 96 °C. The red oily solid then melts from 138 to 155 °C. HR-MS (MALDI+ FT-ICR): m/z = 1246.3977 [M$^{•+}$], calcd for [C$_{70}$H$_{86}$S$_{10}$]$^{•+}$ m/z = 1246.3931. ^{1}H NMR (500 MHz, CDCl$_3$): δ = 7.92 (br. s, 1H), 7.83 (s, 2H), 7.81 (d, J = 1.2 Hz, 1H), 7.80 (d, J = 1.2 Hz, 1H), 7.76 (d, J = 7.8 Hz, 1H), 7.76 (d, J = 7.8 Hz, 1H), 7.68 (br. d, J = 7.6 Hz, 1H), 7.66 (d, J = 8.5 Hz, 2H), 7.64 (d, J = 8.5 Hz, 2H), 7.55 (br. d, J = 7.6 Hz, 1H), 7.48 (dd, J = 7.8, 1.2 Hz, 1H), 7.47 (dd, J = 7.8, 1.2 Hz, 1H), 7.43 (t, J = 7.6 Hz, 1H), 3.01−2.91 (m, 8H), 1.79−1.68 (<m, 8H), 1.53−1.43 (m, 8H), 1.39 (s, 18H), 1.36−1.30 (m, 16H), 0.92−0.86 (m, 12H). ^{13}C NMR (126 MHz, CDCl$_3$): δ = 142.4, 142.3, 138.8, 138.6, 138.3, 138.3, 138.0, 137.9, 137.8, 137.1, 137.1, 137.0, 136.9, 136.4, 136.0, 135.3, 135.3, 133.3, 131.5, 129.0, 128.9, 128.7, 128.6, 127.7, 127.3, 124.5, 124.5, 121.8, 121.6, 121.0, 121.0, 119.7, 114.2, 46.2, 46.1, 36.9, 36.8, 31.6, 31.5, 31.2, 30.0, 30.0, 30.0, 29.9, 28.5, 28.5, 22.8, 22.7, 14.2, 14.2 (14

C's masked). Anal. Calcd for $C_{70}H_{86}S_{10}$: C, 67.37; H, 6.95. Found: C, 67.43; H, 7.02.

Compound 6. To an argon-flushed solution of **15** (49 mg, 39 μmol) in toluene (15 mL) was added AcCl (1.5 mL). The mixture was cooled to 0 °C, and BBr_3 (0.15 mL, 1 M in CH_2Cl_2, 0.15 mmol) was added, resulting in a color change to black. After 3 h, more BBr_3 (0.15 mL, 1 M in hexanes, 0.15 mmol) was added. After 1.5 h, the solution was poured onto ice and extracted with CH_2Cl_2 (3 × 100 mL). The combined organic phases were dried over Na_2SO_4 and concentrated in vacuo. The crude mixture was purified by crystallization from $CHCl_3$/heptane to give **6** as an orange solid (38 mg, 79%). Mp: from 142−150 °C the solid turns red and becomes oily. The red oily solid then melts from 187−190 °C. HR-MS (MALDI+ FT-ICR): m/z = 1218.2891 $[M^{\bullet+}]$, calcd for $[C_{66}H_{74}O_2S_{10}]^{\bullet+}$ m/z = 1218.2890. ^{1}H NMR (500 MHz, C_6D_6): δ = 8.33 (br. s, 1H), 8.33 (br. s, 1H), 8.20 (d, J = 1.5 Hz, 1H), 8.19 (d, J = 1.5 Hz, 1H), 8.04 (dd, J = 1.8, 1.8 Hz, 1H), 7.84 (d, J = 7.8 Hz, 1H), 7.83 (d, J = 7.8 Hz, 1H), 7.72 (d, J = 8.4 Hz, 2H), 7.69 (ddd, J = 7.7, 1.8, 1.1 Hz, 1H), 7.51 (d, J = 8.4 Hz, 2H), 7.49 (dd, J = 7.8, 1.5 Hz, 1H), 7.46 (dd, J = 7.8, 1.5 Hz, 1H), 7.41 (ddd, J = 7.7, 1.8, 1.1 Hz, 1H), 7.23 (t, J = 7.7 Hz, 1H), 2.85−2.77 (m, 6H), 2.74 (t, J = 7.3 Hz, 2H), 1.98 (s, 3H), 1.94 (s, 3H), 1.67−1.54 (m, 8H), 1.38−1.11 (m, 24H), 0.90−0.83 (m, 12H). ^{13}C NMR (126 MHz, C_6D_6, 1:4): δ = 192.3, 192.2, 143.7, 143.5, 139.1, 139.1, 139.1, 139.0, 138.7, 138.6, 137.9, 137.8, 137.6, 137.4, 136.2, 135.4, 133.6, 132.9, 130.3, 129.9, 129.7, 129.6, 128.5, 127.3, 125.2, 122.5, 122.3, 122.0, 121.9, 120.3, 37.0, 36.9, 36.8, 36.6, 31.8, 31.7, 31.7, 30.2, 30.2, 30.2, 29.9, 29.8, 28.7, 28.6, 23.0, 23.0, 14.3, 14.3 (16 C's masked). Anal. Calcd for $C_{66}H_{74}O_2S_{10}$: C, 64.98; H, 6.11. Found: C, 64.87; H, 6.02.

ASSOCIATED CONTENT

Ⓢ Supporting Information

The Supporting Information is available free of charge on the ACS Publications website at DOI: 10.1021/acs.joc.6b01579.

> Additional details and data on the conductance measurements, NMR spectra, differential pulse voltammograms, and X-ray crystallographic data (PDF)
> X-ray data for compound **9b** (CIF)

AUTHOR INFORMATION

Corresponding Authors
*E-mail: h.s.j.vanderzant@tudelft.nl.
*E-mail: mbn@chem.ku.dk.

Notes
The authors declare no competing financial interest.

ACKNOWLEDGMENTS

REFERENCES

(1) (a) Robertson, N.; McGowan, C. A. *Chem. Soc. Rev.* **2003**, *32*, 96−103. (b) Weibel, N.; Grunder, S.; Mayor, M. *Org. Biomol. Chem.* **2007**, *5*, 2343−2353. (c) Kaliginedi, V.; Moreno-García, P.; Valkenier, H.; Hong, W.; García-Suárez, V. M.; Buiter, P.; Otten, J. L. H.; Hummelen, J. C.; Lambert, C. J.; Wandlowski, T. *J. Am. Chem. Soc.* **2012**, *134*, 5262−5275.

(2) (a) Wei, Z.; Li, T.; Jennum, K.; Santella, M.; Bovet, N.; Hu, W.; Nielsen, M. B.; Bjørnholm, T.; Solomon, G. C.; Laursen, B. W.; Nørgaard, K. *Langmuir* **2012**, *28*, 4016−4023. (b) Parker, C. R.; Wei, Z.; Arroyo, C. R.; Jennum, K.; Li, T.; Santella, M.; Bovet, N.; Zhao, G.;

Hu, W.; van der Zant, H. S. J.; Vanin, M.; Solomon, G. C.; Laursen, B. W.; Nørgaard, K.; Nielsen, M. B. *Adv. Mater.* **2013**, *25*, 405−409.

(3) Parker, C. R.; Leary, E.; Frisenda, R.; Wei, Z.; Jennum, K. S.; Glibstrup, E.; Abrahamsen, P. B.; Santella, M.; Christensen, M. A.; Della Pia, E. A.; Li, T.; Gonzalez, M. T.; Jiang, X.; Morsing, T. J.; Rubio-Bollinger, G.; Laursen, B. W.; Nørgaard, K.; van der Zant, H.; Agrait, N.; Nielsen, M. B. *J. Am. Chem. Soc.* **2014**, *136*, 16497−16507.

(4) Fock, J.; Leijnse, M.; Jennum, K.; Zyazin, A. S.; Paaske, J.; Hedegård, P.; Nielsen, M. B.; van der Zant, H. S. J. *Phys. Rev. B: Condens. Matter Mater. Phys.* **2012**, *86*, 235403.

(5) Lee, J. T.; Chae, D.-H.; Ou, Z.; Kadish, K. M.; Yao, Z.; Sessler, J. L. *J. Am. Chem. Soc.* **2011**, *133*, 19547−19552.

(6) Frisenda, R.; Gaudenzi, R.; Franco, C.; Mas-Torrent, M.; Rovira, C.; Veciana, J.; Alcon, I.; Bromley, S. T.; Burzuri, E.; van der Zant, H. S. J. *Nano Lett.* **2015**, *15*, 3109−3114.

(7) García, R.; Herranz, M. Á.; Leary, E.; González, M. T.; Bollinger, G. R.; Bürkle, M.; Zotti, L. A.; Asai, Y.; Pauly, F.; Cuevas, J. C.; Agraït, N.; Martín, N. *Beilstein J. Org. Chem.* **2015**, *11*, 1068−1078.

(8) Christensen, M. A.; Parker, C. R.; Sørensen, T. J.; de Graaf, S.; Morsing, T. J.; Brock-Nannestad, T.; Bendix, J.; Haley, M. M.; Rapta, P.; Danilov, A.; Kubatkin, S.; Hammerich, O.; Nielsen, M. B. *J. Mater. Chem. C* **2014**, *2*, 10428−10438.

(9) (a) Meisner, J. S.; Ahn, S.; Aradhya, S. V.; Krikorian, M.; Parameswaran, R.; Steigerwald, M.; Venkataraman, L.; Nuckolls, C. *J. Am. Chem. Soc.* **2012**, *134*, 20440−20445. (b) Batra, A.; Meisner, J. S.; Darancet, P.; Chen, Q.; Steigerwald, M. L.; Nuckolls, C.; Venkataraman, L. *Faraday Discuss.* **2014**, *174*, 79−89.

(10) Usta, H.; Risko, C.; Wang, Z.; Huang, H.; Deliomeroglu, M. K.; Zhukhovitskiy, A.; Facchetti, A.; Marks, T. *J. Am. Chem. Soc.* **2009**, *131*, 5586−5608.

(11) (a) Moore, A. J.; Bryce, M. R. *Tetrahedron Lett.* **1992**, *33*, 1373−1376. (b) Rybácek, J.; Rybácková, M.; Høj, M.; Belohradsky, M.; Holy, P.; Kilså, K.; Nielsen, M. B. *Tetrahedron* **2007**, *63*, 8840−8854.

(12) (a) Sallé, M.; Belyasmine, A.; Gorgues, A.; Jubault, M.; Soyer, N. *Tetrahedron Lett.* **1991**, *32*, 2897−2900. (b) Lorcy, D.; Carlier, R.; Robert, A.; Tallec, A.; Le Maguerès, P.; Ouahab, L. *J. Org. Chem.* **1995**, *60*, 2443−2447. (c) Frère, P.; Skabara, P. J. *Chem. Soc. Rev.* **2005**, *34*, 69−98. (d) Chen, G.; Mahmud, I.; Dawe, L. N.; Daniels, L. M.; Zhao, Y. *J. Org. Chem.* **2011**, *76*, 2701−2715.

(13) González, M. T.; Leary, E.; García, R.; Verma, P.; Herranz, M. Á.; Rubio-Bollinger, G.; Martín, N.; Agraït, N. *J. Phys. Chem. C* **2011**, *115*, 17973−17978.

(14) Lissau, H.; Frisenda, R.; Olsen, S. T.; Jevric, M.; Parker, C. R.; Kadziola, A.; Hansen, T.; van der Zant, H. S. J.; Nielsen, M. B.; Mikkelsen, K. V. *Nat. Commun.* **2015**, *6*, 10233.

(15) (a) Mayor, M.; Weber, H. B.; Reichert, J.; Elbing, M.; von Hänisch, C.; Beckmann, D.; Fischer, M. *Angew. Chem., Int. Ed.* **2003**, *42*, 5834−5838. (b) Solomon, G. C.; Herrmann, C.; Hansen, T.; Mujica, V.; Ratner, M. A. *Nat. Chem.* **2010**, *2*, 223−228. (c) Arroyo, C. R.; Tarkuc, S.; Frisenda, R.; Seldenthuis, J. S.; Woerde, C. H. M.; Eelkema, R.; Grozema, F. C.; van der Zant, H. S. J. *Angew. Chem., Int. Ed.* **2013**, *52*, 3152−3155. (d) Valkenier, H.; Guédon, C. M.; Markussen, T.; Thygesen, K. S.; van der Molen, S. J.; Hummelen, J. C. *Phys. Chem. Chem. Phys.* **2014**, *16*, 653−662. (e) Manrique, D. Z.; Huang, C.; Baghernejad, M.; Zhao, X.; Al-Owaedi, O. A.; Sadeghi; Kaliginedi, V.; Hong, W.; Gulcur, M.; Wandlowski, T.; Bryce, M. R.; Lambert, C. J. *Nat. Commun.* **2015**, *6*, 6389.

(16) Perrin, M. L.; Burzurí, E.; van der Zant, H. S.J. *Chem. Soc. Rev.* **2015**, *44*, 902−919.

(17) Liang, W.; Shores, M. P.; Bockrath, M.; Long, J. R.; Park, H. *Nature* **2002**, *417*, 725−729.

(18) van der Wiel, W. G.; De Franceschi, S.; Elzerman, J. M.; Tarucha, S.; Kouwenhoven, L. P.; Motohisa, J.; Nakajima, F.; Fukui, T. *Phys. Rev. Lett.* **2002**, *88*, 126803.

(19) Kubatkin, S.; Danilov, A.; Hjort, M.; Cornil, J.; Brédas, J.-L.; Stuhr-Hansen, N.; Hedegård, P.; Bjørnholm, T. *Nature* **2003**, *425*, 698−701.

(20) (a) Leary, E.; Higgins, S. J.; van Zalinge, H.; Haiss, W.; Nichols, R. J.; Nygaard, S.; Jeppesen, J. O.; Ulstrup, J. *J. Am. Chem. Soc.* **2008**,

130, 12204−12205. (b) Liao, J.; Agustsson, J. S.; Wu, S.; Schönenberger, C.; Calame, M.; Leroux, Y.; Mayor, M.; Jeannin, O.; Ran, Y.-F.; Liu, S.-X.; Decurtins, S. *Nano Lett.* **2010**, *10*, 759−764.